K2 photometry and HERMES spectroscopy of the blue supergiant *ρ* Leo: rotational wind modulation and low-frequency waves

C. Aerts,[1,2]★ D. M. Bowman,[1] S. Símon-Díaz,[3,4] B. Buysschaert,[1,5] C. Johnston,[1] E. Moravveji,[1] P. G. Beck,[3,4] P. De Cat,[6] S. Triana,[1,6] S. Aigrain,[7] N. Castro,[8] D. Huber[9,10,11,12] and T. White[12]

[1]*Instituut voor Sterrenkunde, KU Leuven, Celestijnenlaan 200D, B-3001 Leuven, Belgium*
[2]*Department of Astrophysics/IMAPP, Radboud University Nijmegen, NL-6500 GL Nijmegen, the Netherlands*
[3]*Instituto de Astrofísica de Canarias, E-38200, La Laguna, Tenerife, Spain*
[4]*Departamento de Astrofísica, Universidad de La Laguna, E-38205, La Laguna, Tenerife, Spain*
[5]*LESIA, Observatoire de Paris, PSL Research University, CNRS, Sorbonne Universités, UPMC Univ. Paris 06, Univ. Paris Diderot, Sorbonne Paris Cité, France*
[6]*Royal Observatory of Belgium, Ringlaan 3, B-1180 Brussels, Belgium*
[7]*Oxford Astrophysics, University of Oxford, Denys Wilkinson Building, Keble Rd, Oxford, OX1 3RH, UK*
[8]*Astronomy Department, University of Michigan, 311 West Hall, 1085 S. University Ave., Ann Arbor, MI 48109-1107, USA*
[9]*Institute for Astronomy, University of Hawaii, 2680 Woodlawn Drive, Honolulu, HI 96822, USA*
[10]*Sydney Institute for Astronomy (SIfA), School of Physics, University of Sydney, NSW 2006, Australia*
[11]*SETI Institute, 189 Bernardo Avenue, Mountain View, CA 94043, USA*
[12]*Stellar Astrophysics Centre, Department of Physics and Astronomy, Aarhus University, Ny Munkegade 120, DK-8000 Aarhus C, Denmark*

ABSTRACT

We present an 80-d long uninterrupted high-cadence *K2* light curve of the B1Iab supergiant *ρ* Leo (HD 91316), deduced with the method of halo photometry. This light curve reveals a dominant frequency of $f_{\rm rot} = 0.0373\,{\rm d}^{-1}$ and its harmonics. This dominant frequency corresponds with a rotation period of 26.8 d and is subject to amplitude and phase modulation. The *K2* photometry additionally reveals multiperiodic low-frequency variability ($<1.5\,{\rm d}^{-1}$) and is in full agreement with low-cadence high-resolution spectroscopy assembled during 1800 d. The spectroscopy reveals rotational modulation by a dynamic aspherical wind with an amplitude of about $20\,{\rm km\,s}^{-1}$ in the Hα line, as well as photospheric velocity variations of a few $\rm km\,s^{-1}$ at frequencies in the range 0.2–$0.6\,{\rm d}^{-1}$ in the Si III 4567 Å line. Given the large macroturbulence needed to explain the spectral line broadening of the star, we interpret the detected photospheric velocity as due to travelling superinertial low-degree large-scale gravity waves with dominant tangential amplitudes and discuss why *ρ* Leo is an excellent target to study how the observed photospheric variability propagates into the wind.

Key words: asteroseismology – techniques: photometric – techniques: spectroscopic – stars: massive – stars: oscillations – stars: rotation.

1 INTRODUCTION

Blue supergiants are in the least understood stage of the evolution of massive stars. Lack of understanding of this stage is unfortunate, since the successors of these stars play a key role in the chemical evolution of their host galaxy. The nucleosynthetic yields after the blue supergiant stage are strongly dependent on the helium core mass at the onset of hydrogen shell burning and how the material gets mixed in the stellar interior during the pre-supernova evolution (e.g. Heger, Langer & Woosley 2000; Langer 2012). It would thus be highly beneficial if blue supergiant variability could be monitored and exploited in terms of the interior physical properties, just as it has recently become possible for evolved low- and intermediate-mass stars from asteroseismology (Bedding et al. 2011; Mosser et al. 2014; Aerts, Van Reeth & Tkachenko 2017b). For blue supergiants, this requires uninterrupted high-precision space photometry covering months to years, but such data sets are scarce.

Long-term ground-based photometry of mmag-level precision (e.g. van Genderen 1989; Lamers et al. 1998, and references therein) and spectroscopy of $\rm km\,s^{-1}$ precision (e.g. Markova et al. 2005; Simón-Díaz et al. 2010; Kraus et al. 2015; Martins et al. 2015)

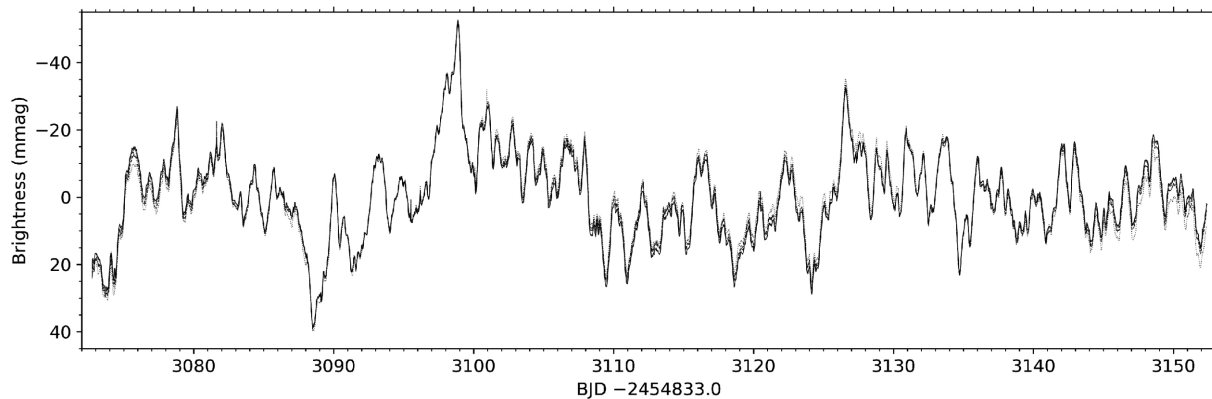★ E-mail: conny.aerts@ster.kuleuven.be

Figure 1. Four versions of the light curve of ρ Leo, based on the four different halo masks shown in Fig. A1, are overplotted in different line styles. The curves barely show differences, excluding other sources of variability in the masks.

devoted to blue supergiants typically had sparse sampling and led to aliasing and high noise levels in the Fourier spectra. As a result, the interpretation of blue supergiant variability from ground-based data remained limited. Ultraviolet space spectroscopy was found to be more useful in this respect. Indeed, time series spectroscopy from the International Ultraviolet Explorer revealed narrow and discrete absorption components due to rotational modulation and wind variability in the line profiles of blue supergiants (Prinja & Howarth 1986; Massa et al. 1995). Moreover, the low-cadence mmag-precision *Hipparcos* photometry led to the detection of coherent gravity-mode oscillations in some blue supergiants (Lefever, Puls & Aerts 2007).

With the availability of high-cadence μmag-level precision space photometry, a new era has begun for the detection and interpretation of blue supergiant variability. The few earliest data sets revealed large diversity in behaviour and periodicities, making it clear that the search for optimal asteroseismology targets among blue supergiants is challenging (Lefèvre et al. 2005; Saio et al. 2006; Moffat et al. 2008; Aerts et al. 2010; Moravveji et al. 2012; Aerts et al. 2013). A step forward was achieved from combined *Kepler* photometry and long-term high-resolution spectroscopy of the O9.5Iab star HD 188209 (Aerts et al. 2017a). These data revealed low-frequency photospheric variability due to travelling gravity waves, propagating into the wind. A similar study for the more evolved B1Ia supergiant HD 2905 had to rely on low-cadence *Hipparcos* photometry and ground-based spectroscopy and revealed similar variability (Simón-Díaz et al. 2018), although the wind behaviour is more dominant for that star.

In this paper, we report the detection of low-frequency variability in *K2* halo photometry of the bright blue supergiant ρ Leo (HD 91316, B1Iab, V = 3.87). We also performed HERMES spectroscopy of the star with the aim to assess its asteroseismic potential. We present the target in Section 2, each of the two new data sets in Sections 3 and 4, and discuss our interpretation of ρ Leo's variability in Section 5.

2 THE TARGET ρ LEO

In their sample study of blue supergiants, Crowther, Lennon & Walborn (2006) obtained the following stellar parameters of ρ Leo: $T_{\rm eff} \simeq 22\,000$ K, $\log g \simeq 2.55$, $M \simeq 18\,{\rm M}_\odot$, $R \simeq 37\,{\rm R}_\odot$, $\dot{M} \simeq 4 \times 10^{-6}\,{\rm M}_\odot\,{\rm yr}^{-1}$. Recently, Kholtygin & Sudnik (2016) concluded from a 3.5 h high-cadence time series of high-precision high-resolution spectroscopy that the star reveals non-radial

oscillations. Moreover, these authors deduced that the variability signatures due to these oscillations propagate into the wind of the star.

In their extensive spectroscopy study of OB stars, Simón-Díaz & Herrero (2014) found ρ Leo to have $v \sin i = 50$ km s^{-1} and a large macroturbulent line-broadening of 72 km s^{-1}. Such large macroturbulence is naturally explained by multiperiodic large-scale tangential velocity fields in the photosphere (Aerts et al. 2009). The star was included in the MiMeS survey to search for a surface magnetic field (Wade et al. 2016), but these data led to a null detection at the level of a few Gauss (Neiner, private communication) and exclude surface magnetism as an explanation of the macroturbulence.

3 *K2* HALO PHOTOMETRY

Following the idea of scattered-light *Kepler* photometry of the blue supergiant HD 188209 in the nominal Field-of-View of the mission (Aerts et al. 2017a), the technique of halo photometry was developed and is meanwhile well established for the follow-up *K2* mission (Pope et al. 2016; White et al. 2017). We hence proposed ρ Leo for *K2* halo photometry during Campaign 14 of the mission. The *K2* data set of ρ Leo consists of long-cadence (29.4 min) data covering 79.64 d.

We used the *K2* pixel data as provided in MAST[1] and deduced halo photometric light curves by adopting four different masks. The four custom halo aperture masks were constructed from the stacked images, where the saturated pixels centred on the star, as well as the very outer regions, were avoided. We considered the four masks shown in Fig. A1 in Appendix A. Each of the four customised apertures was kept fixed to deduce four versions of the light curve. This photometry was subsequently passed through the K2SC software package (Aigrain et al. 2015; Aigrain, Parviainen & Pope 2016; Aigrain et al. 2017) to correct for the pixel drifts and their related instrumental effects. An outlier rejection was applied to this photometry and we finally corrected for a long-term (instrumental) trend by means of a linear polynomial. The four versions of the light curve, with the *K2* flux transformed to brightness expressed in mmag, are overplotted in Fig. 1. They are almost indistinguishable from each other. Given the very different masks, we are confident that the halo photometry reveals the variability of ρ Leo itself and is not contaminated by any other source. The *K2* data set has a time

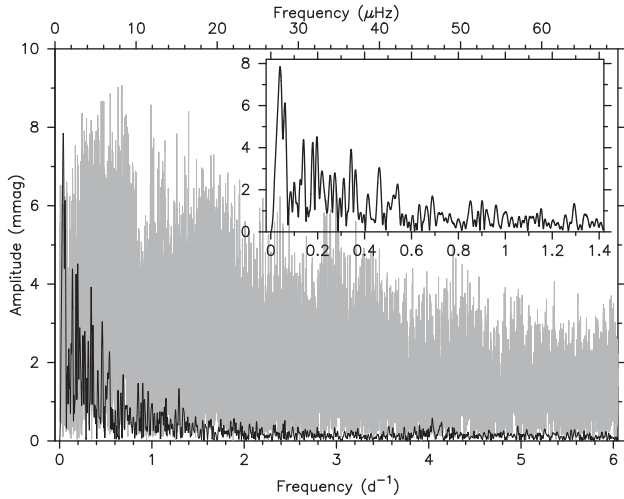[1] archive.stsci.edu/kepler/data_search/search.php

Figure 2. Scargle amplitude spectra of the *K2* halo (thick black lines) and *Hipparcos* (thin grey line) photometry of ρ Leo.

base of 79.64 d, leading to a frequency resolution (Rayleigh limit) of 0.0126 d^{-1}.

All frequency analyses of the four light curves shown in Fig. 1 give the same conclusions; in the rest of this paper, we show the results for the full line in Fig. 1 based on the mask in the upper left-hand panel of Fig. A1. Scargle amplitude spectra of the *K2* and *Hipparcos* photometry are shown in Fig. 2. No significant variability due to the star is detected above 6 d^{-1}. It can be seen that the *Hipparcos* data were of insufficient quality to detect ρ Leo's photometric variability, but that the *K2* data reveals periodic signal. The dominant frequency occurs at $f_1 = 0.0397 \pm 0.0002$ d^{-1} with an amplitude of 7.94 ± 0.28 mmag. The statistical frequency error is far below the uncertainty due to the low resolving power of 0.0126 d^{-1}. An unresolved secondary frequency peak closer than the Rayleigh limit to f_1 occurs, in addition to numerous unresolved low-amplitude frequencies.

Fig. 3 shows a short-term Fourier-transform (STFT) for the *K2* data. Each of the colour-coded stacked Fourier transforms are over-sampled by a factor of 10. A moving time-step of 1 d and a window size of 30 d was used to create this STFT, but the result is independent of this particular choice. It can be seen that f_1 exhibits amplitude and frequency modulation. This is also the case for other frequency peaks. Due to the Rayleigh limit, we are unable to distin-

guish intrinsic amplitude and frequency modulation of one feature from multiperiodic beating due to unresolved frequencies. Hence, any pre-whitening procedure may introduce spurious signal in the residuals, given the unresolved nature of f_1 and its harmonics. For this reason, we first turn to sparse but long-term spectroscopy to improve upon the value of f_1, before interpreting the *K2* halo photometry further.

4 HERMES SPECTROSCOPY

We included ρ Leo in an ongoing long-term spectroscopic monitoring program (Simón-Díaz et al. 2015) to assemble multi-instrument data similar to those used in the study of HD 188209 (Aerts et al. 2017a) and HD 2905 (Simón-Díaz et al. 2018). Here, we limit our analysis to the currently available 293 spectra taken with the HERMES spectrograph (Raskin et al. 2011) attached to the 1.2-m Mercator telescope at La Palma Observatory, which covers a time base of 1800 d (Rayleigh limit of 0.0006 d^{-1}). Given the mmag variability of ρ Leo, we have intensified the ongoing spectroscopic monitoring to reach higher cadence, but the current HERMES data are sufficient to refine the dominant frequencies of the star.

In this initial paper, we focus on the equivalent width (EW) and radial velocity $\langle v \rangle$ of the photospheric line Si III 4567 Å and the Hα wind line to demonstrate that different mechanisms are responsible for the variability in these regions of the envelope and atmosphere of ρ Leo. We use these two line diagnostics to highlight that similar variability to that in the *K2* photometry is also present in the low-cadence optical spectroscopy. These two quantities are computed as the zeroth- and first-order moments of the lines, where EW captures temperature variations and $\langle v \rangle$ centroid velocity variations (Aerts, de Pauw & Waelkens 1992). Figs 4 and 5 show the only 'dense' part of these otherwise sparsely sampled data and reveal (quasi-)periodicity. The Hα line, formed at the base of the stellar wind, shows complex and large-amplitude variations with a dominant time-scale of $\sim$30 d in $\langle v \rangle$ and about half this period in EW. To further demonstrate the variability in Hα, we show 20 epochs of spectroscopic observations in Fig. 6, which vary between strong absorption and weak emission. The time-scale and amplitude of this variability differ to that of the photospheric Si III 4567 Å line, which can also be seen in Figs 4 and 5.

Just as in Simón-Díaz et al. (2018, their fig. 6), we studied the variability of the zeroth and first moments of various lines formed in the photosphere in addition to Si III 4567 Å. Even though our spectroscopic monitoring of the star is still ongoing, the current
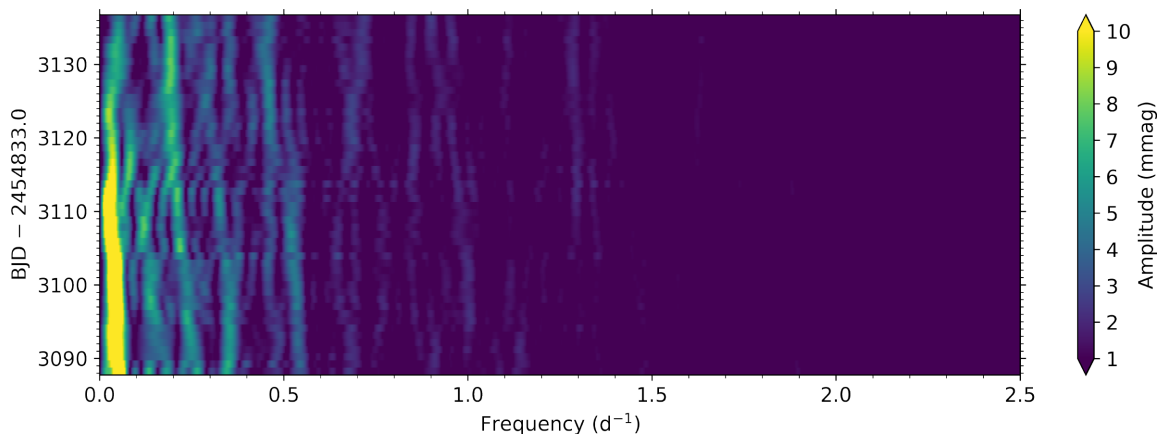

Figure 3. STFT of the *K2* halo light curve computed for a moving time step of 1 d and with a window size of 30 d.
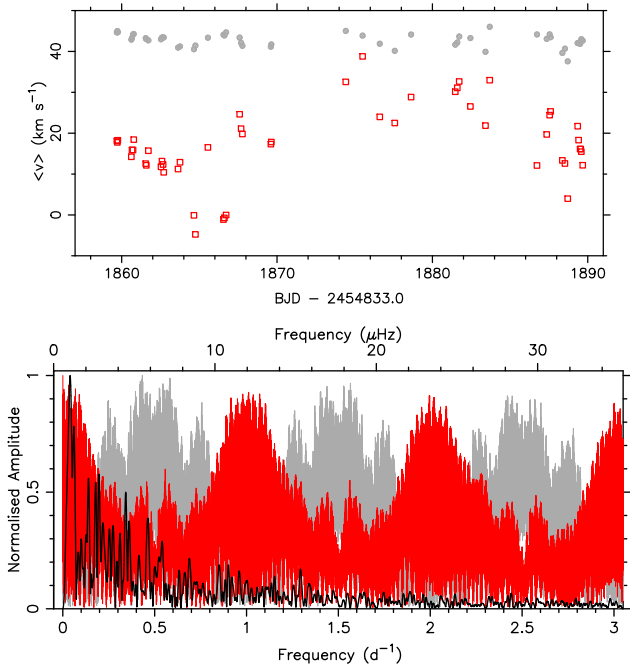
Figure 4. Top panel: excerpt of the HERMES radial-velocity data computed as the first moment of the Si III 4567 Å line (grey circles) and H α (red squares). Bottom panel: Scargle spectra normalized to maximal amplitude for the *K2* data (black) and of the HERMES ⟨*v*⟩ for the Si III 4567 Å line (grey) and H α (red).
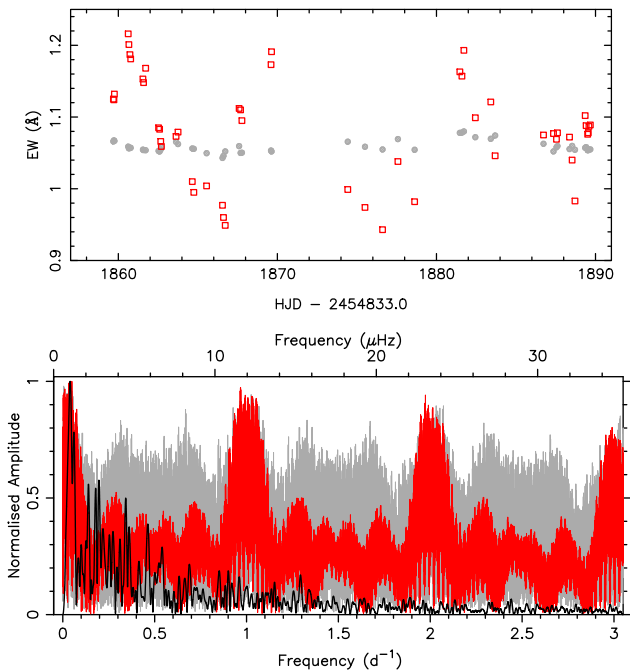

Figure 5. Top panel: excerpt of the HERMES EW data computed as the zeroth moment of the Si III 4567 Å line (grey circles, arbitrarily shifted by 0.7 Å for visibility purpose) and H α (red squares). Bottom panel: Scargle spectra normalized to maximal amplitude for the *K2* data (black) and of the HERMES EW for the Si III 4567 Å line (grey) and H α (red).
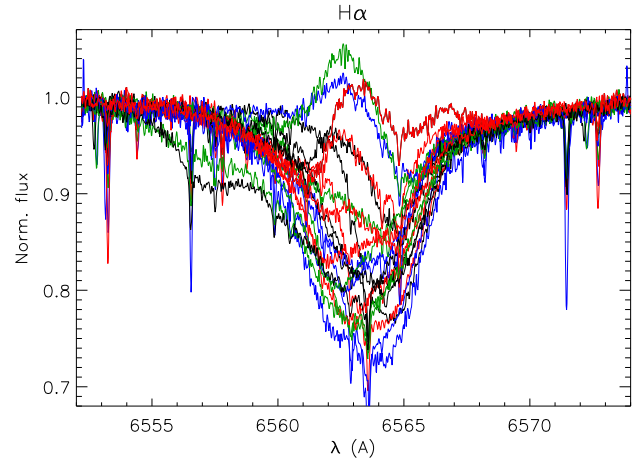

Figure 6. Line profile variability of H α for 20 epochs varying between strong line absorption and weak line emission.
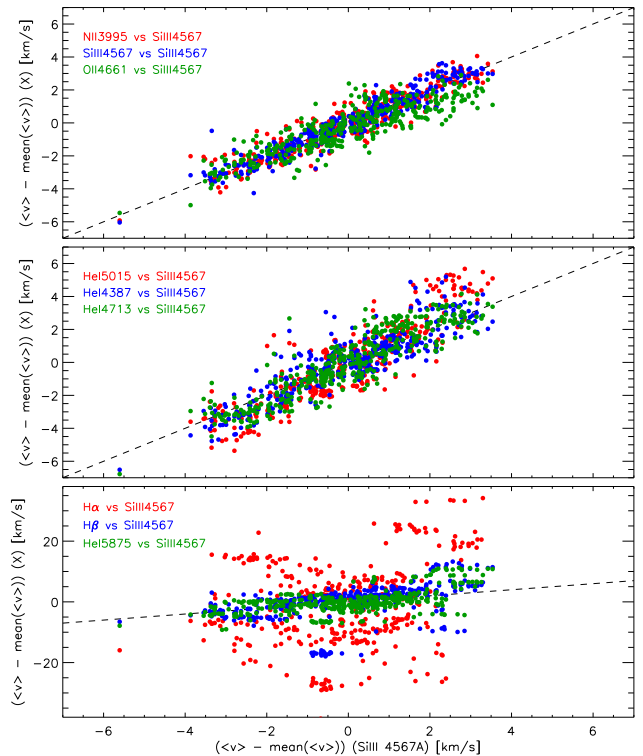

Figure 7. Correlations in the temporal variability of the first moment (centroid) of various diagnostic lines of ρ Leo. The Si III 4567 Å line is used as baseline as indicated by the axis labels. Top and middle panel: photospheric lines formed at similar depth than the baseline; bottom panel: lines formed at the base of the wind. The dashed lines in each panel represent the bisector.

HERMES spectroscopy already reveals that the moments of various photospheric lines are strongly correlated with each other, as illustrated in Fig. 7. Similar coherent periodicity was found in photospheric lines of the early-B supergiant HD 2905 (Simón-Díaz et al. 2018). Furthermore, we investigated the zeroth and first moment variability of other lines partially formed in the wind, including H β and H γ, and found that their variability is different from the one of the photospheric lines (see also Fig. 7). This indicates that the dynamic wind of ρ Leo alters the observed variability in the photosphere, again as in HD 2905 (Simón-Díaz et al. 2018). A more
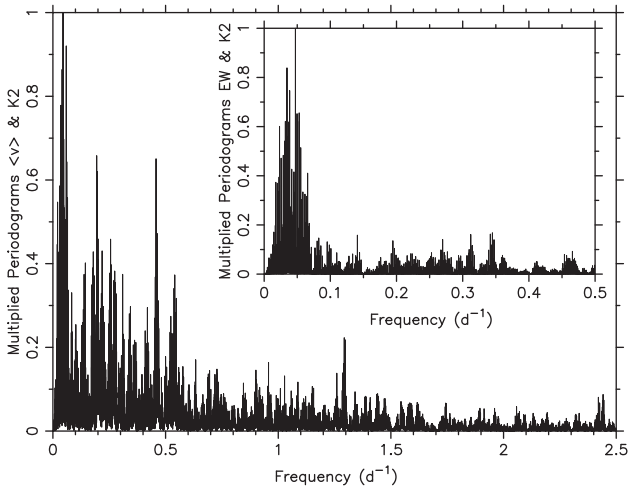
Figure 8. Multiplied Scargle spectra of the *K2* halo photometry of ρ Leo with its $\langle v \rangle$ (and EW: inset) of the Hα and Si III 4567 Å lines of the HERMES spectra.

Figure 9. Amplitude and phase modulation of the dominant frequency across the *K2* light curve.

detailed analysis using continuing but higher-cadence spectroscopy will be provided in a future follow-up paper. For the purposes of the present paper, the photospheric line Si III 4567 Å and the Hα wind line are fully representative and sufficient to probe the variability mechanism in the photosphere and wind of ρ Leo.

We now turn to the Fourier analysis of the EW and $\langle v \rangle$ of the Si III 4567 Å and the Hα lines. Scargle amplitude spectra of these four full data sets are heavily affected by daily aliasing but the EW of both lines are dominated by a frequency close to f_1 and $2f_1$, within the Rayleigh limit of the *K2* data. This is also the case for the Hα $\langle v \rangle$ data; the Si $\langle v \rangle$ data indicate a dominant low-amplitude ($\simeq$1.6 km s^{-1}) frequency near $\simeq$0.43 d^{-1}. In each of the individual data sets, these frequencies reach low significance, typically between 2 and 4σ.

As in Aerts et al. (2017a), we exploit the full potential of the totally independent *K2* and HERMES data sets by 'merging' the information in the Fourier domain. This is done by computing harmonic geometric means of the normalized dimensionless individual Scargle amplitude spectra, where we give equal weight to the *K2*, Hα, and Si III 4567 Å data. In this way, we combine the high-cadence uninterrupted *K2* data with time base of 80 d with the low-cadence aliased HERMES photospheric and wind data with time base of 1800 d. This has the aim to illustrate which frequencies are present in the multiple data sets, but we refrain from any formal statistical interpretation in terms of significance. The result is shown in Fig. 8 and leads to a dominant frequency based on EW of $f_{\rm rot} = 0.0373$ d^{-1}, well within the *K2* Rayleigh limit of f_1. The dominant frequency for $\langle v \rangle$ is slightly different. This is not surprising as it is determined by the velocity rather than the temperature variations in the photosphere. As this frequency gives a much poorer fit to the *K2* data, we select the frequency on the basis of EW and interpret $f_{\rm rot}$ as the best estimate of the rotation frequency of the star (with corresponding rotation period of 26.8 d). Harmonics of $f_{\rm rot}$ occur in both the $\langle v \rangle$ and EW multiplied Scargle amplitude spectra. The latter confirm the findings based on the *K2* data alone and revealed by Fig. 3: the dominant *K2* frequency is due to cyclic variabillity caused by rotational modulation by an aspherical stellar wind and reveals fine structure due to a variable amplitude and frequency. This is illustrated quantitatively in Fig. 9, where we show the amplitude and phase of $f_{\rm rot}$ computed from the *K2* data following the methodol-
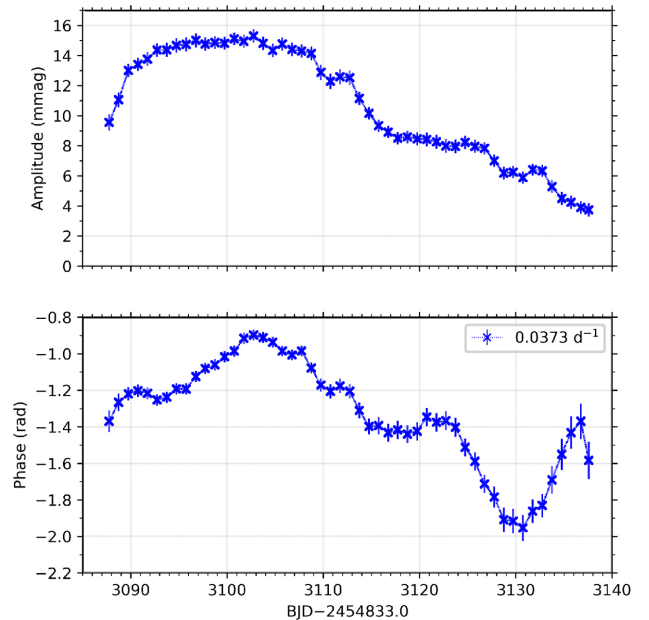
ogy of Bowman et al. (2016). The figure represents the amplitude and phase of $f_{\rm rot}$ by tracking them at fixed frequency using 30-d time bins with a 1-d moving time-step. Values of amplitude and phase were optimised using linear least-squares fits in each time bin and plotted against time. The zero-point of the time-scale for the phases is BJD 2454943.0. Results are qualitatively similar for other combinations of bin duration and overlap, but Fig. 9 represents the best compromise between frequency and temporal resolution in the STFT.

The $\langle v \rangle$ multiplied amplitude spectrum in Fig. 8 reveals two more frequencies that stand out beyond the fine structure of the rotational frequency: $f_2 = 0.1956$ d^{-1} and $f_3 = 0.4588$ d^{-1}. These hardly occur in the EW spectrum nor in the individual Scargle spectrum of the Hα $\langle v \rangle$. These two frequencies are therefore interpreted as due to velocity variations in the photosphere. Both of them also occur in the *K2* data, at low amplitude. This suggests a different astrophysical cause compared to $f_{\rm rot}$ and we interpret these frequencies, along with several others in Fig. 8 that peak above 0.2, in Fig. 3, as due to gravity waves – whether this photospheric variability is caused by coherent gravity-mode oscillations or convectively driven travelling gravity waves, or a combination thereof, cannot be deduced from the *K2* data due to the too limited time base of 80 d. The frequency spectra derived from numerical simulations of gravity waves in massive stars have a similar morphology to that shown in Fig. 8 (Rogers et al. 2013; Aerts & Rogers 2015; Aerts et al. 2017a; Simón-Díaz et al. 2018), which supports this interpretation as the cause of the photospheric variability in ρ Leo. Furthermore, ρ Leo lies within the parameter space of the instability strip on the Hertzsprung–Russell diagram, in which high-degree coherent gravity-mode oscillations are predicted (Star 'C' in fig. 3 of Godart et al. 2017). Gravity waves have dominant tangential amplitudes, which we observe for ρ Leo in spectroscopy of the photospheric lines, supporting this interpretation. For either the case of travelling gravity waves or coherent gravity modes, our detection of the photospheric variability using both high-quality *K2* space photometry combined with high-resolution spectroscopy

is in full agreement with the similar detection by Kholtygin & Sudnik (2016).

5 INTERPRETATION AND DISCUSSION

We unravelled the dominant causes of the variability of the blue supergiant ρ Leo from combined 80 d *K2* halo photometry and 1800 d high-resolution spectroscopy. All variability occurs at frequencies below 1.5 d^{-1}. We find that the dominant variability is caused by rotational modulation at the base of the aspherical stellar wind, with amplitudes of about 8 mmag in photometry and 20 km s^{-1} in velocity as revealed by H α (Figs 1, 4, and 5). Variability with amplitudes below 2 km s^{-1} in velocity and 4 mmag in brightness are connected with velocity and temperature variations in the photosphere. These low-amplitude variations are interpreted as due to gravity waves caused by convective driving or by an opacity mechanism in the envelope. This interpretation relies on the large macroturbulent velocity measured in the spectral line wings of the star, which requires tangential rather than vertical velocity fields. The velocity variations occur at frequencies that are an order of magnitude higher than the rotation frequency, indicating superinertial large-scale waves of low degree.

The tangential velocities associated with convectively-driven gravity waves in the stellar photosphere of massive stars are of order a tenth of a km s^{-1} for an individual wave (Rogers et al. 2013), but the combined effect of hundreds of gravity waves is similar to the effect of a few coherent heat-driven gravity-mode oscillations (Aerts & Rogers 2015). Thus, both travelling gravity waves and coherent gravity modes are feasible explanations for the variability observed in the *K2* space photometry and high-resolution HERMES spectroscopy of ρ Leo, which is similar to the conclusions made recently for other O and B supergiants (Aerts et al. 2017a; Simón-Díaz et al. 2018) and previously for ρ Leo by Kholtygin & Sudnik (2016).

Besides the studies of HD 188209 (O9.5Iab) and HD 2905 (B1Ia), combined long-term space photometry and high-resolution spectroscopy was recently also assembled for the fast rotator ζ Puppis (spectral type O4I(n)fp, Ramiaramanantsoa et al. 2017). The BRITE photometry revealed cyclic variability at the base of the stellar wind with a rotation period of 1.78 d, as well as stochastic low-amplitude variability assigned to sub-surface convection. A quantitative comparison between the frequency spectra caused by convection/granulation velocities must await 3D convection simulations in the envelope of OB stars. 2D numerical simulations of gravity waves do lead to the appropriate horizontal velocity fields that explain macroturbulence (Aerts et al. 2009; Aerts & Rogers 2015), but this must yet be proven for velocities due to convection. A key question is whether surface convection can give rise to large-scale tangential velocity fields in the appropriate frequency range.

Should convective motions cause the detected variability, one also expects some level of granulation to occur in addition to stochastic variability, as is the case for acoustic waves excited in the envelope of red giants. Using the approximation of granulation scales from Kallinger & Matthews (2010) for the mass, radius and T$_{eff}$ estimates for ρ Leo, and assuming that the solar values can be scaled, leads to granulation signal at frequencies $\lesssim$1.5 d^{-1}. With the current *K2* data set at hand, we cannot explicitly rule out near-surface convection and granulation as (one of) the causes of the detected multiperiodic variability of ρ Leo. However, the shape of the detected frequency spectrum is more in line with gravity waves, because we see isolated frequency peaks that resemble a discrete spectrum of eigenvalues of the star.

We are currently in the process of obtaining further high-resolution and high-cadence spectroscopy of ρ Leo. In a follow-up study, we will carry out a detailed quantitative analysis of various spectral lines that are formed at different depths in the photosphere and in the wind. This will allow the derivation of the tangential versus vertical velocity structure, as well as how the photospheric variability, concluded to be non-radial gravity-modes oscillations by Kholtygin & Sudnik (2016) and/or travelling gravity waves in this work, propagates into the wind. The wind in ρ Leo is clearly a dynamic and turbulent environment, as indicated by the line profile variability of H α shown in Fig. 6 varying between strong absorption and emission. Furthermore, the variability of other lines formed partially in the wind (i.e. H β and H γ) vary differently with smaller amplitudes than that of H α but larger than those of pure photospheric lines. Therefore, ρ Leo is a promising target to investigate how photospheric variability propagates into the wind (see e.g. Kholtygin & Sudnik 2016).

Our study once more illustrates the power of combined high-cadence uninterrupted space photometry with a time base of months and ground-based high-resolution spectroscopy covering several years. Such a combination is necessary for a proper interpretation of hot supergiant variability and the hunt for optimal asteroseismic targets among blue supergiants.

REFERENCES

Aerts C., Rogers T. M., 2015, ApJ, 806, L33

Aerts C., de Pauw M., Waelkens C., 1992, A&A, 266, 294

Aerts C., Puls J., Godart M., Dupret M.-A., 2009, A&A, 508, 409

Aerts C et al., 2010, A&A, 513, L11

Aerts C et al., 2013, A&A, 557, A114

Aerts C et al., 2017a, A&A, 602, A32

Aerts C., Van Reeth T., Tkachenko A., 2017b, ApJ, 847, L7

Aigrain S., Hodgkin S. T., Irwin M. J., Lewis J. R., Roberts S. J., 2015, MNRAS, 447, 2880

Aigrain S., Parviainen H., Pope B. J. S., 2016, MNRAS, 459, 2408

Aigrain S., Parviainen H., Roberts S., Reece S., Evans T., 2017, MNRAS, 471, 759

Bedding T. R. et al., 2011, Nature, 471, 608

Bowman D. M., Kurtz D. W., Breger M., Murphy S. J., Holdsworth D. L., 2016, MNRAS, 460, 1970

Crowther P. A., Lennon D. J., Walborn N. R., 2006, A&A, 446, 279

Godart M., Simón-Díaz S., Herrero A., Dupret M. A., Grötsch-Noels A., Salmon S. J. A. J., Ventura P., 2017, A&A, 597, A23

Heger A., Langer N., Woosley S. E., 2000, ApJ, 528, 368

Kallinger T., Matthews J. M., 2010, ApJ, 711, L35

Kholtygin A. F., Sudnik N. P., 2016, MNRAS, 458, 1604

Kraus M. et al., 2015, A&A, 581, A75

Lamers H. J. G. L. M., Bastiaanse M. V., Aerts C., Spoon H. W. W., 1998, A&A, 335, 605

Langer N., 2012, ARA&A, 50, 107

Lefever K., Puls J., Aerts C., 2007, A&A, 463, 1093

Lefèvre L et al., 2005, ApJ, 634, L109

Markova N., Puls J., Scuderi S., Markov H., 2005, A&A, 440, 1133

Martins F., Marcolino W., Hillier D. J., Donati J.-F., Bouret J.-C., 2015, A&A, 574, A142

Massa D et al., 1995, ApJ, 452, L53

Moffat A. F. J. et al., 2008, ApJ, 679, L45

Moravveji E., Guinan E. F., Shultz M., Williamson M. H., Moya A., 2012, ApJ, 747, 108

Mosser B et al., 2014, A&A, 572, L5

Pope B. J. S. et al., 2016, MNRAS, 455, L36

Prinja R. K., Howarth I. D., 1986, ApJS, 61, 357

Ramiaramanantsoa T. et al., 2017, MNRAS, 473, 5532

Raskin G et al., 2011, A&A, 526, A69

Rogers T. M., Lin D. N. C., McElwaine J. N., Lau H. H. B., 2013, ApJ, 772, 21

Saio H et al., 2006, ApJ, 650, 1111

Simón-Díaz S., Herrero A., 2014, A&A, 562, A135

Simón-Díaz S., Herrero A., Uytterhoeven K., Castro N., Aerts C., Puls J., 2010, ApJ, 720, L174

Simón-Díaz S. et al., 2015, in Cenarro A. J., Figueras F., Hernández-Monteagudo C., Trujillo Bueno J., Valdivielso L., eds, Highlights of Spanish Astrophysics VIII. p 576

Simón-Díaz S., Aerts C., Urbaneja M. A., Camacho I., Antoci V., Fredslund Andersen M., Grundahl F., Pallé P. L., 2018, A&A, preprint (arXiv:1711.08994),

van Genderen A. M., 1989, A&A, 208, 135

Wade G. A. et al., 2016, MNRAS, 456, 2

White T. R. et al., 2017, MNRAS, 471, 2882

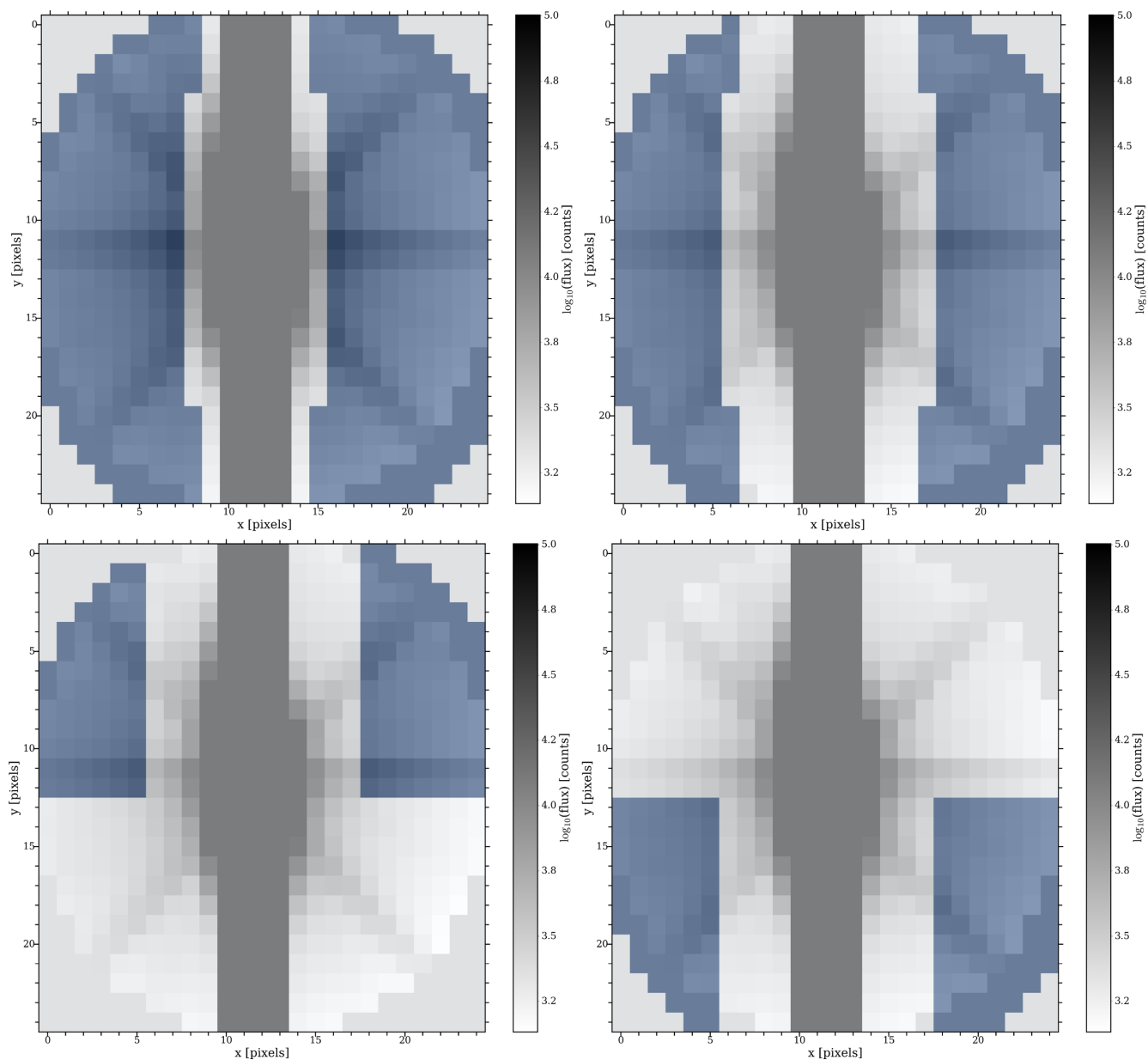## APPENDIX A: ADDITIONAL FIGURES: *K2* MASKS USED FOR THE LIGHT CURVE EXTRACTION

Figure A1. The four investigated halo masks used for the light curve extraction of *K2* photometry of ρ Leo are shown in blue in each panel, which do not include saturated pixels. The chosen mask is shown in the top left-hand panel with the extracted light curve corresponding to the full line in Fig. 1.

This paper has been typeset from a TEX/LATEX file prepared by the author.